NASA CR 151943

John Foster & Associates, Inc.
485 Arboleda Dr.
Los Altos, Calif. 94022

(NASA-CR-151943) EFFICIENT COMPUTER ALGORITHMS FOR INFRARED ASTRONOMY DATA PROCESSING (Foster (John) and Associates, Inc.) 80 p HC A05/MF A01 CSCL 09B
N77-16780
Unclas
G3/61 11520

EFFICIENT COMPUTER ALGORITHMS

FOR

INFRARED ASTRONOMY DATA PROCESSING

A

Technical Approach Report

by

Robert F. Pelzmann, Jr., Ph.D.

November 30, 1976

JAN 1977
RECEIVED
NASA STI FACILITY
INPUT BRANCH

Prepared under Contract No. NAS2-9432

for

National Aeronautics and Space Administration

TABLE OF CONTENTS

		Page No.
1.0	INTRODUCTION	1
2.0	DATA FROM INFRARED OBSERVATIONS	2
2.1	Infrared Astronomical Measurement Techniques	3
2.1.1	Ground-Based Infrared Measurements	3
2.1.2	Space-Based Infrared Measurements	6
2.2	Sample Data Streams	8
2.3	Classification of Infrared Source Data	17
3.0	DATA PROCESSING FOR POINT SOURCES	19
3.1	Sequencing of the Data Processing Task	19
3.2	Noise Analysis	23
3.3	Detection Techniques	32
3.4	Weighting Functions	39
3.5	False Source Algorithms	47
4.0	DATA PROCESSING FOR EXTENDED SOURCES	54
4.1	Slightly-Extended Objects	54
4.2	Photometric Mapping	56
4.3	Detection of Extended Emission	62
5.0	DATA PROCESSING SYSTEMS	65
5.1	Overall Structure	65
5.2	Front-end Processing Flow	70
5.3	Back-end Cascade	72
5.4	Extended Sources and Survey Calibration	75
6.0	REFERENCES	77

LIST OF ILLUSTRATIONS

Figure		Page No.
1	Sample Data - Three Color Star Measurement	10
2	Sample Data - Small Extended Object	14
3	Sample Data - Complex Extended Object	15
4	Point Source Processing Sequence	21
5	Sample Data - Radiation Spikes with Crosstalk	49
6	Sample Data - Dust Particle Signatures	51
7	Computing Structure	66
8	Back-End Cascade Structure	74

1.0 INTRODUCTION

This report will outline the data processing techniques to be studied for use in infrared astronomy data analysis systems. The ensuing investigation will be restricted to consideration of data from space-based telescope systems operating as survey instruments. Resulting algorithms, and in some cases specific software, will be applicable for use with the Infrared Astronomy Satellite (IRAS) and the Shuttle Infrared Telescope Facility (SIRTF). Operational tests will be made during the investigation using data from the Celestial Mapping Program (CMP). The overall task is somewhat different from that involved in ground-based infrared telescope data reduction.

Section 2.0 reviews the characteristics of space-based survey data and the differences between that and ground-based data. Sections 3.0 and 4.0 then discuss the processing task needed for point sources and extended sources, respectively. Section 5.0 considers the overall software/hardware data processing system involved, and Section 6.0 concludes this report with a reference list including a number of representative texts related to the data processing task.

2.0 DATA FROM INFRARED OBSERVATIONS

This section reviews the techniques of infrared astronomical measurement and the resulting data streams. Included are descriptions of representative space survey systems and the resulting data collected by one of them. A three-level division of infrared source data is described based on the divergence in data processing approaches created by physical differences in the astronomical sources.

The application of the data reduction techniques discussed in this report is limited for the most part to the processing of survey measurements. A primary requirement of survey analysis is the discovery of unknown but physically real infrared sources and the determination of their positions and intensities. Other photometric studies, on the other hand, are intended to measure to high accuracy the intensities and spectral characteristics of known sources. Survey data is intrinsically statistical in nature in that a tradeoff occurs between the accuracy of a measurement (existence, position, intensity), the observation schedule, and the data processing techniques, which gives a non-zero false detection rate for maximum information transfer. Optimizing this information on the basis of some defined set of criteria is the goal of the data processing system and has direct implications on the design of the sensor.

2.1 Infrared Astronomical Measurement Techniques

Infrared astronomical measurements are essentially photometric in nature rather than image-oriented. That is, a measurement of the infrared radiation from a specific direction is made by a collection of mechanical, optical, and electrical components, which results in an electrical signal related to the incident infrared intensity. The temporal sequence implicit in this electrical signal is produced by some induced variation in the infrared illumination on the detectors. Most ground-based infrared astronomical systems utilize controlled optical beam switching which alternately illuminates the detector(s) with the radiation from two different regions. Most space-based systems utilize directional scanning to illuminate the detectors with radiation from a sequence of positions. A number of variations on these two approaches is used, and applications are not exclusively ground- or space-based for one or the other, but two different types of data streams result from the described approaches. This report will directly address the processing task for the second data gathering technique. For comparison, however, a general approach to beam switching data gathering follows.

2.1.1 Ground-Based Infrared Observations

Ground-based telescopes realize beam switching by oscillating one of the telescope's optical components, usually the secondary mirror of a Cassegrain telescope. The modulation frequency is chosen either for optimum detector response or to minimize the

effects of spatial and temporal variations in atmospheric emission. Small fields of view and small beam separations are used to minimize the effects of this sky noise. Such an approach allows high accuracy in photometric measurement but strongly discriminate against extended sources or low brightness gradients, and also is at odds with survey requirements of rapid area coverage.

Further, these oscillating secondary mirrors and detector dewars are commonly installed on telescopes initially designed for visual photography. The secondary oscillation commonly induces a signal due to side-lobe emissions of the telescope structure which limits the system performance level. This is partially treated by using undersized secondary mirrors, thus wasting some fraction of the collected photons. An oscillating primary mirror was used in the 2.2 micron survey of Neugebauer and Leighton[1] to avoid this difficulty.

The modulated radiation is transferred to a cryogenic detector, passing through one or more spectral filters. It is common to use two filters, one acting as the window to the cryogenic dewar and a second one internal to the dewar, cooled to the detector temperature to reduce the thermal emission from it to the detector. Even with this approach the radiant flux within the spectral bandpass is dominantly sky photons and the detector materials are restricted to high background flux

types. This is because the detector always sees either bright sky or bright sky plus dim stars in a beam switching system.

The square wave signal from the detector is amplified by a low-noise A.C. coupled amplifier mounted within or immediately outside the dewar assembly. For either case, a load resistor is usually mounted on the cold sink within the dewar to minimize its thermal noise. The signal is then rectified by a phase-locked amplifier synchronized to the secondary mirror oscillations and integrated until the signal-to-noise ratio has reached an acceptable level.

The measured voltage is then calibrated by observing standard stars shortly before or after the experimental measurement. These standards are chosen to be nearby the measurement to minimize the effects of air mass and directional variations in atmospheric transmission. Positions are determined from the outputs of the setting circles of the telescope and from offsets of known stars.

A number of aspects of this approach limits the usefulness for sky surveying. To achieve some uniformity in survey operation the telescope is generally scanned slowly with the dwell time of a star on a detector determining the integration period and defining the sensitivity limit. In this manner, the Neugebauer-Leighton survey stretched over a period of three years measuring almost 5600 sources in a declination band between -33° and +81° brighter than 2.5×10^{-15} watts cm^{-2} μm^{-1} at 2.2 μm. An attempt

to survey at 11 μm was made by Low,[2, 3] observing in a narrow spectral window of the atmosphere. His best results were at a sensitivity of 2×10^{-16} watts cm^{-2} μm^{-1} at a rate of 3.8 square degrees per hour. This implies a period of two years for single-measurement coverage of a major fraction of the sky.

Even accepting a very slow rate of coverage and unimpressive sensitivity, ground-based surveys are limited by their inability to discover even slightly extended objects. A number of sources extending 4 to 5 arc minutes located by a sounding rocket survey are unmeasurable by current ground-based telescopes even when photographic identification of some of the sources has been made.

Finally, data analysis in these systems is currently a manual task, and extensive system expansions would be needed to make even the collection of position and brightness information automatic. Furthermore, to channel this data into computer systems capable of handling the complexity and size of the data analysis task would make such an effort unacceptably costly in both dollars and facilities for such limited scientific output. No further discussion of ground-based systems or data processing will be made except for occasional fortuitous transfers from space survey systems and the techniques used on their data.

2.1.2 Space-Based Infrared Measurements

When a survey instrument is raised above the atmosphere, tremendous gains are realized in capability and simplicity. The background photon flux and sky noise are eliminated, and

measurements can be made in spectral regions inaccessible to ground-based telescopes. Furthermore, since frosting is not a problem in space, the entire telescope system can be cooled to greatly reduce the background from the instrument itself. Under such low background conditions, infrared detectors exhibit very high detectivities. The very short time constants of these detectors permit high scan rates for temporal frequency selection eliminating the complexities of oscillating components. The AFGL Infrared Celestial Survey Program[4, 5, 6] is representative of previous space survey efforts and is described below.

The AFGL survey was performed using a small cryogenically cooled sounding rocket-borne telescope. The instrument was a 16.5 cm diameter folded Gregorian equipped with internal baffles and aperture stops to minimize side-lobe response and radiation from the telescope structure with all optical components cooled by liquid helium to around 15°K. Interference filters selectively isolated different portions of the linear staggered detector array along the direction scan. This permitted almost simultaneous measurements in three spectral bands with effective wavelengths of 4.2, 11.0, and 19.8 μm with bandwidths of 1.5, 5.1, and 5.6 μm, respectively.

The field-of-view for each detector was 3.4 arc minutes in the scan direction and 10.5 arc minutes in the cross scan direction. To insure complete scan coverage each detector was overlapped

by adjacent elements in each color. This reduced the effective spatial resolution to 3.4 by 7.1 arc minutes for the non-overlapped portion and 3.4 by 1.7 arc minutes for the overlapped portion.

The telescope was yoke-mounted in a rocket fixed alt-azimuth coordinate system. During the flight the telescope azimuth axis was actively fixed in celestial coordinates to within 12 arc seconds by means of a visual star tracker coupled to a cold gas attitude control reaction system. The zenith position of the telescope line of sight was read to ±30 arc seconds by a digital optical encoder mounted on that axis. Azimuthal positions were obtained from the output of a visual stellar aspect sensor and scan rate gyro to 1 arc minute.

Infrared sources transiting a detector generated electrical signals which were then amplified, bandlimited, sampled, digitized, and transmitted to the ground on a PCM telemetry link. Simultaneously, the outputs of the position control sensors were sampled, digitized, and merged with the detector data in the telemetry link. Time tags were added to the data from a crystal controlled reference clock at the ground station.

2.2 Sample Data Streams

To illustrate the complexity of the data processing task, several examples of raw data from a space survey are presented. Interpretation of these data records is aided by an understanding of the focal plane layout. There are eight detectors in each

of three groups, each group measuring a different spectral region. For a given cross scan position one detector in each color is used, separated by a small distance in the scanning direction; the eight detectors are slightly overlapped in the cross scan direction. A point source will thus pass through one or two detectors in each color in a single scan producing pulses with a well-defined time lag in successive detectors. Sample data are shown in Figures 1 through 3. Each line is the signal from one detector displayed as a function of scan azimuth (time). For clarity of presentation and interpretation, the records are grouped into triplets of detectors, one in each of three colors; the eight groups are the cross-scan divisions of the detector array. Time and amplitude scales are the same in all figures. One channel of the bottom group is omitted from all figures because that detector was malfunctioning and not considered an element of the survey.

Figure 1 is archetypal of the star survey data task. Prominent in the second group from the bottom is the three-color signature from a bright star showing the characteristic time stagger of a real source transit. It is important to note, however, that this is a very strong signal. While the actual signature of a star transit is determined by the focal plane design and the electronics system, the illustrated signal is a typical response of a system optimized for point source detection. The third color measurement here (bottom trace of this group) is to the eye near the limit of detection although

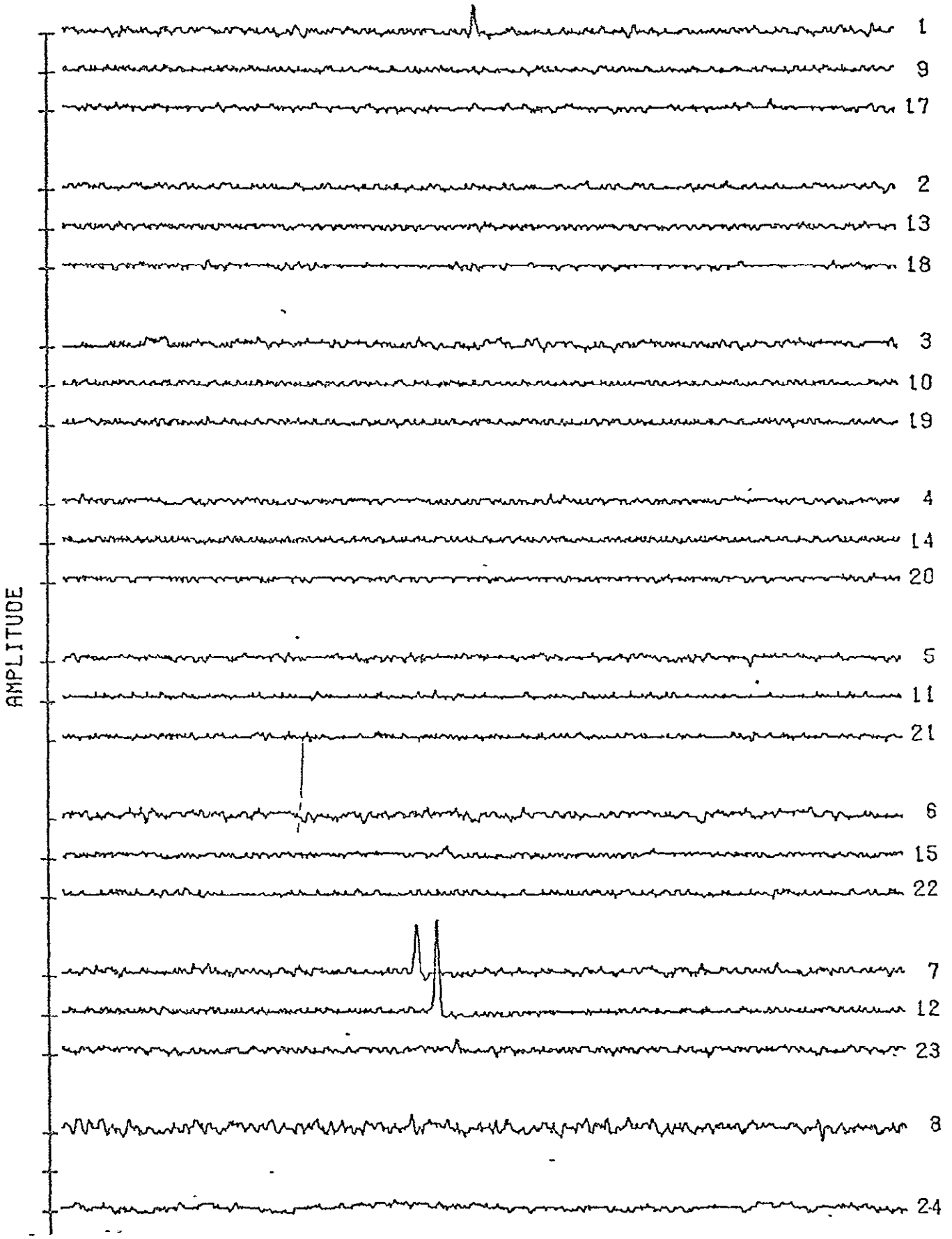

Figure 1. Sample Data - Three Color Star Measurement

its actual peak signal-to-rms noise value is over six. Since statistically significant numbers of real sources can be detected with individual measurements having S/N values as low as three, it is obvious that manual analysis will miss a significant portion of the most interesting sources.

Furthermore, the illustrated data, which is a plot of the digital sample sequence, is oversampled by a factor of four from the minimum necessary to identify a signal at a 90% confidence level. If constraints in another system require a minimum sampling rate, it is fully possible for two consecutive samples to bracket the true signal peak, thus underestimating the peak value by 1/2 the ratio of sample rate and rise time times the digitizing step size. This significantly constrains the photometric accuracy for manual analysis approaches.

On the other hand, numerical detection techniques can be constructed which operate very well at low S/N levels with a false alarm rate which is a smooth function of the noise characteristics. Additionally, numerical methods can easily make best estimates of amplitudes by convolution with model signatures, allowing smaller photometric uncertainties. Secondary analysis and reconfirming observations can then be used to reduce the false alarm rate without losing the real but weak sources that eyeball analysis would always miss.

Many of the noise characteristics of survey data are also in evidence in Figure 1. The noise is the key to source detection, and a thorough understanding of its characteristics is mandatory for efficient data analysis. Of course, the most important elements of the noise character, its amplitude and frequency spectra, are not easily comprehended from the illustration. Those subjects will be covered in later reports.

Several important elements are evident, however. In a number of the traces, the noise amplitude is seen to vary. (This is especially evident if Figures 2 and 3 are also consulted.) This nonstationary amplitude variation implies a variable false alarm rate for fixed detection gates which complicates the task of creating a uniformly complete survey. In some portions of several traces, the signal is seen to go "flat." In these periods the noise has fallen below the digitizing step level and only the noise peaks appear. Such flat segments could lead to anomalously low rms values and further surges in the false source rates. Since it is wise to choose digitizing steps comparable to the noise level for best dynamic range and other considerations, the resulting contribution to the noise character by the digitizing process must be thoroughly accounted for.

A final caveat in the data task is illustrated by the signature in the topmost trace. Here, an apparently strong signal occurs in only one color of the group. This does not have the

character of one of the known types of false signals, yet some anomalies can be noted. First, the signal form is not a true match to a point source signature. Second, although it is very large, no signal is seen in the other two spectral bands. Since the signal is seen on the middle of the three spectral bands, the object must have an extremely nonthermal spectra if it is real. Since the noise is also seen to be variable immediately prior to the signal, there is much uncertainty to be associated with it. Such attributes must be measured in a comprehensive data processing system in order to provide later stage software routines with enough information to make consistent decisions.

Figures 2 and 3 demonstrate the character of extended source data typical of a point-source optimized scanning survey. Seen in Figure 2 in the top four groups of detectors is a compact HII region with a size somewhat less than 30 arc minutes diameter as indicated by the data. Note that the signature in the second detector group is very similar to the point source of Figure 1. Of course, the ratio of intensities is indicative of a low color temperature as could be expected for an HII region. It is clear that the signals from all 12 detectors are related to a single object which would pass most point source criteria. Obviously, care must be taken to note and measure the extended source attributes so that the signals are assigned to only one source and that that source is identified as a small extended object.

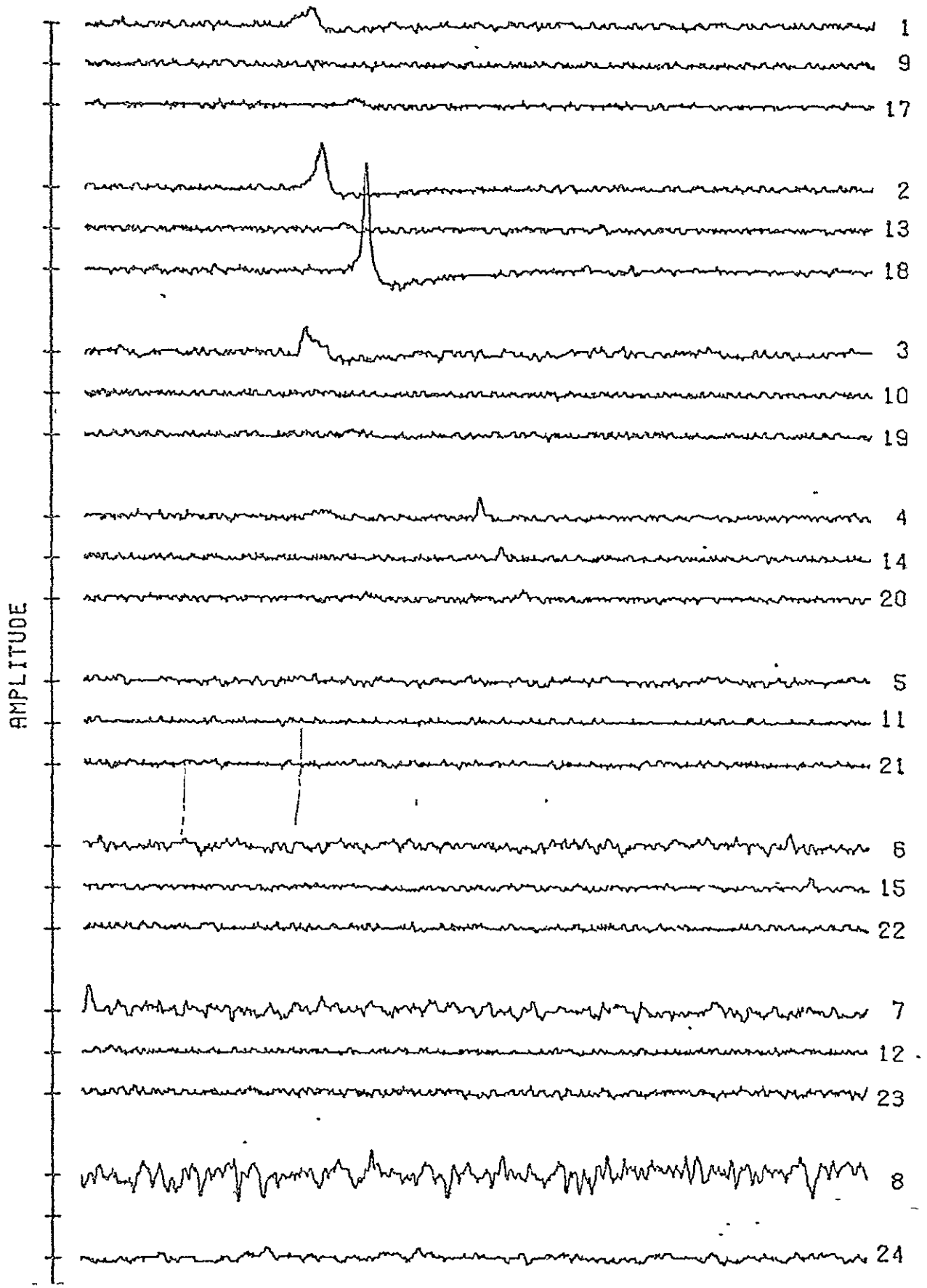

Figure 2. Sample Data - Small Extended Object

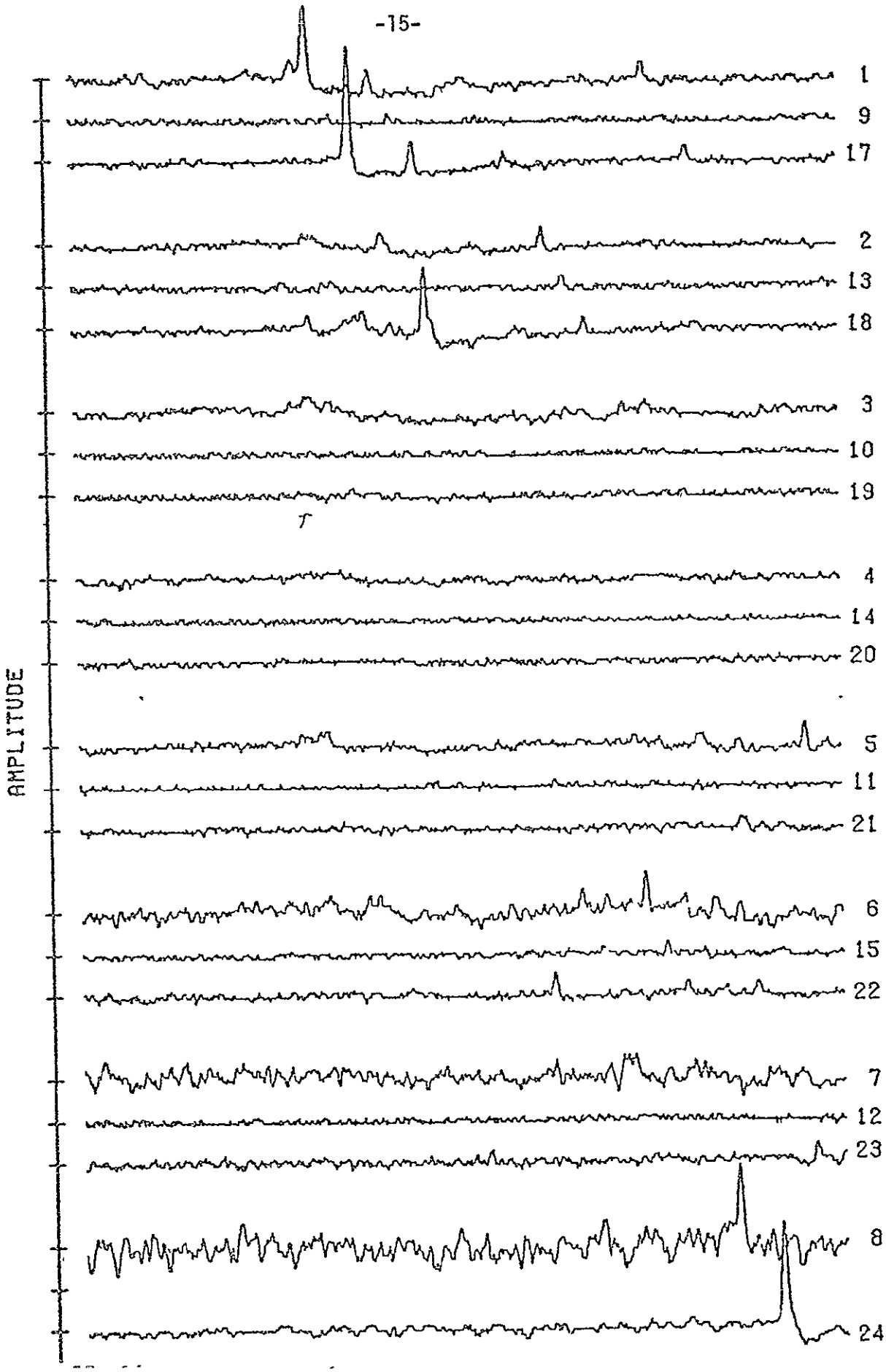

Figure 3. Sample Data - Complex Extended Object

In Figure 3 an example of a much more complex extended source is shown. Keeping in mind that this sensor system is A.C. coupled with strong low frequency de-emphasis, the source structure is seen to cover nearly 6° in azimuth. That it is seen only weakly below the third detector group (zenith measurement) indicates that the source probably extends out of the field of view. Other scans at higher zenith angle may have further data on this source. Because the bandlimiting function of the electronics is well known, it is possible, in principle, to recover some of the low frequency information and reconstruct an intensity map of this object. The techniques for accomplishing this recovery and reconstruction are not well understood but are an element of this study.

A philosophical question is raised by this source on data cataloging. If such complex sources are processed as intensity maps as an addendum to a point-source catalog, how should one treat the obvious hot spots in this object? We may be seeing stars imbedded in a large emission region - should these spots then be included in the point-source catalog as well as the maps? Or should the point-source signature be subtracted from the map and only the extended emission shown? The answers to such questions are of primary importance in the design of the software system, as will be discussed in a later section of this report.

2.3 Classification of Infrared Source Data

The characteristics of the astronomical sources being surveyed divides them into three distinct classes, as demonstrated in the previous section. The three classes are point sources (e.g., stars) with diffraction limited images; slightly extended sources (e.g., compact HII regions) whose signatures are point-like but not diffraction limited; and diffusely extended sources (e.g., the Orion Nebula) with spatial structure extending several degrees.

Point Sources for the purpose of the data analysis system are defined as IR detections with signatures characterized by the optical limit of the telescope system. Generally, this is diffraction limited with the actual image blur a fraction of both the optical components and the spectral characteristics of the filter system and the source. From a data analysis viewpoint, these signals are individually the minimum information content limit of the system. Typically, detector size and basic frequency characteristics are set by the point sources response needs. As such, they place the smallest bandwidth requirement on the signal transmission and processing systems.

Slightly Extended Objects (SEO's) are not much different from point sources. These objects are not too much larger than the detector size, perhaps up to tens of arc minutes. As such, they can normally be handled by point-source processing if

some care is taken in measuring their extent. Since their information content in the data stream does involve a slightly wider bandwidth than true point sources, detection using point-source optimized filters will underestimate their size. Accommodating this extra information is a task of SEO processing.

For source sizes beyond a few tens of arc minutes, the information content of the source signal encompasses a significantly wider bandwidth than point sources, with the increase toward lower frequencies. This increase must be accommodated at all levels of telescope system and data processing design. A goal of such processing might be to produce a map of the region in the form of a photo-image or a contour plot of isophote levels. Because of the distinctly different end product, extended sources might best be processed separately from the point-source system. The only overlap would occur at first detection where the interleaved information of point-like and extended sources is separated. As mentioned, this involves both philosophical questions on how to handle the data and technical ones on how to treat the wideband information.

3.0 DATA PROCESSING FOR POINT SOURCES

This section is concerned with the techniques to be used in detecting and processing point sources. First, the sequence of actions to be implemented in going from raw, time sequence data to an organized final catalog is described. Then follows a discussion of the functional algorithms necessary in the sequence. The most basic function area is detection techniques where three common approaches are described and compared on the basis of gaussian statistics. Noise analysis logically precedes detection, including the technique for measuring noise values and the parameters contributing to its character. Another portion discusses the weighting functions used in various second-stage processing routines. Finally, the algorithms concerned with false sources are discussed.

3.1 Sequencing of Point-Source Processing Routines

A number of different measurements are derived from raw survey data. These values are used to discard false sources from the data base and to control the manner in which repeated observations are weighted and combined. By separating the several decision gates into the proper sequence, the best throughput of data to the final catalog can be achieved. The controlling philosophy in designing this sequence is to make the most critical decisions first. With a goal of cataloging all real sources and no false sources, the first level of detection must be designed for maximum probability of detection, admitting a concurrent maximum in false alarm rate. Given then that all

detectable real sources are included in the detections list, following decisions are sequenced so that at each stage the largest possible amount of false sources are discarded first without affecting the real ones. Stated concisely, the statistical confidence level of the data base as a whole should increase by the largest possible amount following each decision.

Figure 4 diagrams a sequence which analysis and experience with other survey data bases indicates closely approaches that ideal; each step is discussed briefly below In most cases the gates are simple tests on the magnitude of the confidence measure. Other gates are more complex combinations of criteria, such as identifications, background brightness in that direction, and channel performance. The first five gates could even vary as a function of time depending on the variations in sensor performance and background conditions. The last gate might be variable in order to maximize the real star content of the final catalog, but the scientific community generally prefers a catalog with some sort of statistical uniformity, which would mean a fixed gate perhaps at a brightness level corresponding to a 90% confidence of completeness.

The first gate, at step 5 of the sequence, does not discard a large number of the detected signals. However, since it is testing for specific false signals, it has negligible effect on the real ones. Tests performed here are for particle hits (or other rapid-rise phenomenon), telemetry dropouts, and dust particles. Since each of these has a unique signature very

Figure 4. Point-Source Processing Sequence

1	Data Input
2	Noise Analysis and Measurement
3	Detection
4	Measure characteristics of source, determine 1st confidence measure (CM)
5	Discard specific false sources (1st gate)
6	Gate on raw statistics (2nd gate)
7	Combine signals based on focal plane characteristics, re-do CM
8	Gate on FPA anomalies (3rd gate)
9	Combine multiple scans, re-do CM
10	Gate scan anomalies, e.g., moving objects (4th gate)
11	Determine observation record for each source
12	Gate total observation quality of each source (5th gate)
13	Determine positional associations
14	Gate to desired catalog statistics (6th gate)
15	OUTPUT

unlike a real source, they can be easily tested for. Of course, the deleted sources need to be saved as a separate file for reference later and for status monitoring.

The second gate, occurring at step 6, is the first statistical testing of source quality. The detection and measurement steps determined a number of values which are somewhat independent measures of the source signature. For large signals, any one of these would be sufficient to qualify a real measurement; weaker sources pose a more difficult challenge. The values of correlation, S/N, amplitude, and duration are tested to accept or reject a detection. This step should trap a significant fraction of the false detections which pass through a gaussian 3 sigma test statistic. The gate level here will probably show the widest variations with time due to nonstationary noise effects.

The next step combines potential multiple detector signals of some source. The associated gate will delete signals attributable to crosstalk between channels, referring to the lists of false sources for time coincidence testing. Other focal plane effects will also be removed here as they are identified from detailed knowledge of the sensor system.

If additional observations are made in a given area, a very strong gate can be created favoring real sources. With a detailed knowledge of the sensor performance and noise history,

a very high confidence can be attached to sources seen repeatedly. The algorithm for this weighting is discussed in Section 3.4. Sources rejected by this test may be moving objects such as artificial satellites, planets, or asteroids, and could be subjected to further analysis outside the point-source flow.

The remaining steps in the illustrated sequence serve to organize the final data base and catalogs. Decisions and gates here intend to qualify the catalog to some external standards.

3.2 Noise Analysis

The entire data processing scheme is strongly controlled by the noise characteristics. Specifically, noise analysis is needed in two parts of point-source analysis. First, a local "true" rms value of the noise is used as a detection criterion in several possible detection tests. This measurement is somewhat circular since the true noise evaluation must exclude sources, but the sources can't be excluded until they have passed a signal vs. noise detection. Second, a simple rms value does not fully characterize non-gaussian or nonstationary noise. Separate analysis is useful outside the processing flow to understand the amplitude-frequency spectra of the noise, the effects of baseline offsets, the influence of digitization on the noise, and the success of source removal for noise calculations. This detailed analysis should be monitored for

its influence on the multiple decision gates of the processing sequence.

A comment is appropriate on the origins of noise and signal in the data stream. Consider the signal (before the bandlimiting filter and digitizer) as a rectangular pulse of duration τ. Its power spectral density is given by

$$S(w) = \left(\frac{\sin \tau w/2}{\tau w/2}\right)^2 \qquad 3.2\text{-}1$$

which is illustrated below:

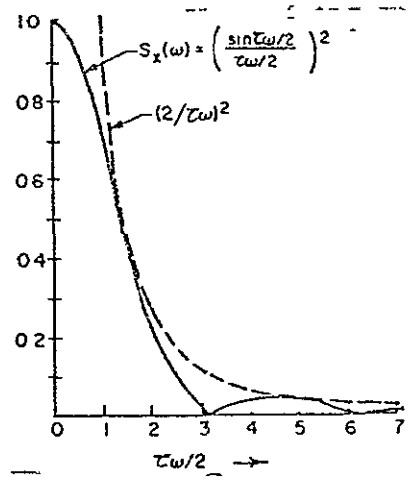

The largest part of the signal's power is near zero frequency. If the noise is white with sharp bandlimits larger than $\tau w/2 = 3$, the signal power-to-noise power ratio decreases as the frequency increases. Then the overall S/N ratio (which is the integral over frequency of the signal PSD ÷ noise PSD) can be improved by removing the higher frequencies. Then the signal power will be reduced only slightly while the noise is reduced more severely. If this "optimizing" filter follows the $\sin^2 x/x^2$ or the $1/x^2$ envelope of the signal's PSD, then the S/N improvement

will be optimal. However, this process tends to make the noise more like the signal so that the cross correlation coefficient of this filtered signal with a model signature becomes large even if no signal is present. This problem is further exacerbated when an A.C. coupled transfer function is used in the sensor for stability reasons. Then the strongest portion of the signal, near zero frequency, is de-emphasized. The low frequency noise is also reduced, but the general effect is to remove a greater portion of the signal power than the noise power. Thus, it is desirable to use the best possible low frequency performance in the sensor system even for the detection of point sources! The problem for extended sources is even worse since when the dwell time τ becomes very large, the first zero in the PSD falls at a very low frequency so that very little of the signal's power exists at the cutoff frequency of the point-source signature.

One should note that the PSD of a rectangular pulse is the same whether the pulse was produced by a detector scanning rapidly over a point source or by a chopped or beam-switched sensor scanning slowly over the star. In the latter case, it is possible to produce several rectangular pulses for a single star (if the chopping rate exceeds the star's dwell time). These multiple signatures can be processed independently or co-added to increase the confidence measure of the detection. However, since such a chopped system is looking at the source only 1/2 of its time, at least two cycles are needed to achieve the same CM as the scanning system. A further difficulty with a beam-switched sensor is the

confusion in the system caused by the presence of a different star in each beam.

In implementing these concepts the realization described below is taken for noise calculation. The noise value itself is used only as a numerical value and is determined only as a voltage. The digitizer number count cannot, in general, be used because the digitizer input is not linearly related to the detector output; rather, some logarithmic compression is typically used in the intermediate amplifiers. All processing then should occur after this compression is inverted.

The noise value itself is calculated using a straightforward rms summation:

$$\sigma^2 = \frac{1}{N-1} \sum_{i=1}^{N} (X_i^2) - \frac{1}{N(N-1)} \left(\sum_{i=1}^{N} x_i \right)^2 \qquad 3.2\text{-}2$$

It can be shown that the effects of a constant value offset over the N samples have no effect on the square deviation. However, any organized change in the mean value of X_i over the N samples easily becomes the dominant element of σ^2. That is, if the mean value drifts linearly over N samples, so that:

$$X_i = Y_i + ai \qquad 3.2\text{-}3$$

then the mean square deviation (MSD) is

$$\sigma^2 = \sigma_y^2 + a^2 \frac{N(N+1)}{12} + \frac{2a}{N-1} \left\{ \sum_{i=1}^{N} iy_i - \frac{N+1}{2} \sum_{i-1}^{N} y_i \right\} \qquad 3.2\text{-}4$$

where σ_y^2 is the true MSD of the data. Obviously, the constant drift heavily weights the noise value through the second term in the above equation. Low frequency baseline drifting of the data, a phenomenon known to occur in IR detector systems, has much the same effect as does the presence of a real source signature.

To compensate for real sources present, the noise value is calculated using continuous blocks of data without stars. This seems somewhat circular, but in practice the blocks containing stars have MSD values much larger than empty noise blocks. By monitoring the noise level over several blocks the star signatures are easily discarded in determining the local average MSD. Alternatively, a low-pass digital filter can be applied to the sequence of MSD values which cuts off this rapid fluctuation in the noise due to source presence. For example,

$$\langle MSD \rangle_i = K\ MSD_i + (1-K)\ \langle MSD \rangle_{i-1} \qquad 3.2\text{-}5$$

where the brackets <> indicate the filtered, or weighted, average value of the noise. The value of K is chosen to provide the appropriate frequency cutoff in the spectrum of MSD values.

The effect of low frequency baseline drifting on the MSD calculation is more difficult to compensate. One approach is to reduce the number of values in a block (the N value) so that the second term in 3.2-4 is acceptably small. Since this

also reduces the confidence of the σ_y^2 determination, an optimum value of N exists which balances the accuracy against the error. Another approach is to apply a high-pass digital filter to the data to remove the low frequency drifting. This may be an optimal filter for point-source discrimination, and hence, an efficient approach to the noise calculation. However, because of the contribution of digitization noise and the possible effects of a nonstationary noise variance, the optimally filtered noise is not uniformly related to the raw noise. This tends to complicate the statistical control of the noise evaluation, balancing off the efficiency of the optimal filter approach for noise calculation. The third possible solution to the drifting baseline is to use a best fit determination to subtract the baseline. By choosing a sufficiently small N, a first order orthogonal fit to the block's data can adequately remove the effects of the second and third terms in 3.2-4.

A key problem of continuous noise measurement is the point in the processing sequence where the MSD is calculated. As will be discussed in Section 3.3, the raw data stream can be transformed into several possible domains. Whether the noise is best determined using the raw data, the optimally filtered data, or the correlated data must be determined from a thorough understanding of the actual instrument performance. The gate level for source detection is then related to the calculated MSD value at a level which corresponds to the desired error rate for

gaussian statistics. This is operationally adjusted by monitoring a detailed analysis of the noise parameters. (Self-adaptive detection schemes skirt the noise analysis issue under certain types of non-ideal noise by continuously compensating the detection algorithm for the noise character.) Most detection schemes assume that the noise is stationary, additive, white, bandlimited and gaussian; more deeply imbedded is the implicit assumpcion that the noise process is random and ergotic. Real noise rarely achieves this ideal state, and accurate control of the performance of the detection scheme requires a knowledge of the deviations from the above standards. The monitoring of this status is the second major function of the noise analysis requirements. To understand these deviations, we begin with a description of the ideal noise. The deviations from this standard will be adapted in Section 3.3 to control the detection techniques.

The data stream is assumed to consist of a pure signal and an additive random noise:

$$r(t) = s(t) + n(t) \qquad 3.2\text{-}6$$

Obviously, we have lumped all elements of r(t) that are not the signal s(t) which we desire to detect into the noise n(t). If part of this noise is a non-random function, the performance of our detection scheme will be degraded; first, the extraneous function will make a significant contribution to the magnitude

of the noise variance, as demonstrated above. Second, and perhaps more significant, the power spectrum of the lumped noise will contain a strongly correlated function, skewing the statistical error rate. Further discussions will assume that this function has been subtracted from the received signal to generate r(t).

Further, we assume that there are no multiplicative noise terms $f[s(t)]\ n(t)$ in 3.2-6. In real infrared sensors, and in photon limited detectors in general, there is always a noise increase in the presence of a signal because of the statistical fluctuations in the photon quanta which are proportional to the root of the photon density. Hence, the noise rises from $n(t)$ to $n(t) + k\sqrt{s(t)}$ when a source is present. In practice, however, the second noise term increases the uncertainty of the amplitude determination not the error rate of the detection. It is not feasible to actually measure the noise in the presence of a signal by subtracting the detected signal because sampling rates used are not high enough to completely determine the signal (100% certainty). The noise is calculated where signals are not detected, and 3.2-6 is assumed to hold so that this value can be transferred to the detection period.

The random noise is said to be stationary if its probability density function is invariant to a shift of the time origin. Then:

$$p(X_t, X_{t-\tau}) = p(X_{t+t'}, X_{t+t'-\tau}) \qquad 3.2\text{-}7$$

The autocorrelation function $R_x(t, t-\tau)$ of the noise is defined as:

$$R_x(t, t-\tau) = \iint X_t \, X_{t-\tau} \, p(X_t, X_{t-\tau}) \, dX_t dX_{t-\tau} \qquad 3.2\text{-}8$$

If 3.2-7 holds, then $R_x(t, t-\tau) = R_x(\tau)$; however, even if 3.2-7 is not true, when the noise has a time invariant mean and $R_x(t, t-\tau) = R_x(\tau)$ then the noise is <u>wide-sense stationary</u>, which is sufficient for all detection techniques requiring stationary noise. Further, when the process is ergotic, then the ensemble average given by 3.2-8 is equal to the time average autocorrelation function,

$$R_x(\tau) = \lim_{T\to\infty} \left(\frac{1}{2T}\right) \int_{-T}^{t} x(t) \, \overset{*}{x}(t-\tau) \, dt \qquad 3.2\text{-}9$$

where the asterisk denotes complex conjugation.

The noise is white when its power spectral density $S_x(w)$ is a constant $(N_0/2)$ over the entire frequency range, and the autocorrelation function is a delta function $(N_0/2)\sigma(\tau)$. Here, the power spectral density is the Fourier transform of the autocorrelation function:

$$S_x(w) = \int_{-\infty}^{\infty} R_x(\tau) \, e^{-iwt} \, d\tau \qquad 3.2\text{-}10$$

When the noise is bandlimited to a range $|w|<\Omega$, then

$$S_x(w) = N_0/2 \quad |w|<\Omega \quad , \quad R_x(\tau) = \frac{N_0\Omega}{2\pi}\frac{\sin\Omega\tau}{\Omega\tau} \qquad 3.2\text{-}11$$

Finally, the gaussian properties of the noise are defined by the probability density function·

$$p(x) = \frac{1}{\sqrt{2\pi}} \; e^{-x^2/2} \qquad 3.2\text{-}12$$

For a digital processing system, there is a contribution to the uncertainty of the signal due solely to the quantization of the signal into discrete steps. The probability density function for this error is uniform over the quantization internal, so that the maximum possible error is one step, E_0. Then for either rounding or truncation, the MSD of the quantization noise is:

$$\sigma_q^2 = \frac{E_0{}^2}{12} \sum_{m=0}^{n} h^2(mT) \qquad 3.2\text{-}13$$

where $h(mT)$ is the time-domain expression of the transfer function. The summation term in 3.2-12 is important when the transfer function is a logarithmic compression where the quantization noise grows with the signal compression.

3.3 Detection Techniques

The simplest method of point-source detection is the visual analysis of strip chart plots of the detector outputs. The

eye is a remarkable analog processor, but it is rarely possible to "see" signals which have a peak signal-to-rms noise value below 5 or 6 because the eye cannot do the rms process very well. For the large data rate of sky surveys, this is an unfeasible approach in any case. The only benefit of eyeball analysis is that with such a low sensitivity, the error rate is very small. A number of digital algorithms have been used in IR surveys which are described below. Performance analysis for each is beyond the scope of this report but is covered in depth in Whalen[7], or Gerlach.[8] Generally, for ideal noise the stored replica correlator or matched filter is optimum; for nonstationary but otherwise ideal noise, adaptive detection techniques such as phase-coherence and wave period correlations achieve lower overall rates. However, the latter are difficult to realize and costly in processing time. Since the signals are wide-sense stationary over fairly long periods T, the adaptive techniques are discussed briefly below only for completeness. The complications of amplitude determination given a detection are mentioned, but error compensation is generally relegated to the weighting functions of later stages of processing as discussed in Section 3.4. The detection processor will be most efficient by concentrating on detection and then making an estimate of the detected amplitude, leaving to the multiple measurement routines the task of statistically controlling the amplitude accuracy.

The simplest analysis test is the peak signal detector. A detection threshold of peak signal-to-rms noise is selected (e.g., 3σ), and

any sample exceeding that level is selected as a signal. The following samples are searched for a maximum until the sample value again falls below the threshold level before another detection search is initiated. It is possible by this technique to choose signals only one sample long so that even with gaussian noise statistics the false detection rate is high. (At 3σ, there will be 13 samples above the threshold in every 1000; at 10σ, there are only 7.5 in 10^{24} false pulses, but the system sensitivity has been severely degraded for real sources, too.)

In general, the IR sensor system is chosen so that both point sources and larger sources are detectable. Then the bandwidth is larger than necessary for the point-source signature, admitting a larger portion of noise power than signal. To rectify this, it is common to digitally bandlimit the data stream to the minimum for point sources. This is done with a recursion filter of the form:

$$y_i = \sum_{k=1}^{m} h_k \, y_{i-k} + \sum_{l=0}^{N} h'_l \, r_{i-l} \qquad 3.3\text{-}1$$

where the coefficients h_k and h'_l are determined from the desired frequency response, as described in Gold and Rader[9, 10], and elsewhere. In digital filters, we are not limited to real filters since all future and past samples are available; we simply replace the l.h.s. of 3.3-1 with y_{i-k} and set some h_k's to zero and we have a "future" looking filter. (Essentially, these filters begin to respond before a signal appears. The reasons for using

them are complex, but basically they make the realization of the desired transfer function into digital form simpler.)

The use of such a filter becomes optimum when the transfer function is chosen with the complete knowledge of the signature of a real source. In this case, the filter is the inverse of the expected signal, hence the filtered data is an optimal matched correlation output. In fact, there is a slight difference between a true correlator and a matched filter, but the digital realization is identical. For an ideal matched filter, the filter function h(t) is the solution to:

$$\int_0^T h_o(z)\ R_n\ (T-z)\ dz = S(T-\tau) \qquad 3.3\text{-}2$$

where T is the period of the expected signal s(t), and $R_n(t)$ is the autocorrelation function of the noise. The presence of $R_n(t)$ has the same effect as a pre-whitening filter when the noise is colored, further, no assumption of gaussian noise character was made in the derivation of 3.3-2 so that the matched filter will be an optimum detector if $h_o(t)$ satisfies the relation for all time, and if the correlation function of the noise is known.

It is important to note that 3.3-2 is a Freedholm equation of the first kind, and exact solutions are obtainable only for a limited class of autocorrelation functions $R_n(t)$. In the case of nonstationary noise, $R_n(t)$ is determined from the locally stationary noise record, and 3.3-2 is solved for the optimal

filter. This is the simplest form of adaptive detectors in digital processing and results in a complicated software package which is very slow in execution. However, such an approach might be implemented piece-wise when some simple monitor calculation signals a significant change in $R_n(t)$.

Given a properly matched filter $h_0(t)$, the data is transformed via 3.3-1, and a threshold crossing detection is performed on the output. As in the simple peak detection approach, the maximum sample is selected to locate the time of the signal. For white noise, the correlator output, y(t), is:

$$y(t) = \int_0^T r(t)\ s(t)dt \qquad 3.3\text{-}3$$

which is a Bayes-best estimate of the unknown amplitude $\hat{A}$, since

$$\hat{A} = \frac{\int_0^T r(t)\ s(t)\ dt}{\int_0^T s^2(t)\ dt} \qquad 3.3\text{-}4$$

and it is assumed that the reference signal s(t) is normalized so that the denominator of 3.3-4 is unity. By extension, the filter output 3.3-1 is the best estimate of $\hat{A}$ with the weighting function $R_n(t)$ accounted for. Note that for white noise, the solution of 3.3-2 as used in 3.3-1 makes 3.3-1 equivalent to 3.3-3.

All of the preceding approaches are variations on the peak detection technique with various forms of signal conditioning

occurring before detection. A second class of detection techniques ignores the peak signal and concentrates on the zero crossings. Since this approach discards amplitude information in favor of signal period and phase detection, it is possible to make statistically independent tests for amplitude (by peak detection techniques) and existence (by wave-period detection). This approach will give the maximum detection probability since all of the knowledge of the signal is being used. However, in IR survey processing the wave-period approach heavily discriminates against even slightly extended sources. Essentially, the zero crossing detectors make assumptions on the source characteristics rather than on the detector response characteristics, and thus are not well suited to the goal of an unbiased survey in any sense.

However, when a specific class of IR objects is to be searched for, the wave-period processor may be an ideal approach since it intrinsically is insensitive to nonstationary noise. This is because a zero crossing detection scheme relys only on the frequency probability distribution, not the amplitude variations. Since a bandlimited system strongly controls the frequency spectrum, the temporal variations in noise amplitude are relatively unimportant. The wave-period technique will be especially fruitful in multicolor surveys when searching for specific color ratios and wavelengths (e.g., cool extended regions, or hot compact clouds). Such goals are outside the general sky survey, however, so the reader is referred to Gerlach[8] for detailed discussion of the wave-period algorithms.

In the interest of computing reduction, a number of approaches to source detection have been tried which involve much less computation than the optimal filter or correlation approach. However, it was found that more fruitful results were achieved by procedural modifications of the correlation technique than by simplistic algorithms. For example, in computing noise, the square variance is determined rather than the rms value since the SQRT function is very slow in execution. Of course, the detection algorithm must be modified to suit the use of the MSD value, but the increased computation here did not exceed the savings in eliminating all SQRT functions.

Another technique successfully tested was the reduction of the sample size of the model function. This savings could be achieved because in one program the sensor sample rate was nearly four times the Nyquist limit (defined as twice the upper frequency limit of the information). A number of averaging and decimation techniques were tested, all of which performed about the same as the full size correlation. This was expected since little further information is added by the excess samples, and also because the limiting noise on some parts of the data was the quantization error. In fact, a three sample slope predictor smoothing function actually had a lower error rate because of a reduction in the noise variance. This was followed by a correlation detector (optimal filter) matched to the smoothed data stream and was very similar to the complete matched filter in overall complexity. However, if detection

methods less complex (and less accurate) than optimal correlation were desirable for other considerations, the decimation-detection approach can save computing time nearly proportional to the decimation level. That is, 3X decimation takes 1/3 processing time. The actual error performance of this concept has yet to be examined. Further, decimation increases the amplitude uncertainty because the number of samples in 3.3-4 drops.

3.4 Weighting Functions

Weighting functions are used in secondary processing stages to combine the values measured in the detection stage to produce an estimate of the true value of the source amplitude given several measurements. They are also used to create a unitary measure of the signal confidence given multiple detections. In a sense, they are also used to determine the existence of multiple measurements in that the positional matching of independent scans is implemented exactly as a unitary weighting function would be.

Amplitude weighting is the most important task since the detection schemes generally ignore photometric accuracy requirements. This results in a wide scatter in the single scan calibration curves. Since the system noise is nonstationary and since the detector response is typically variable over long periods, the best calibration methods involve fitting standard star brightness to measured voltages in a least square sense for each stationary segment of a scan. Thus, secondary uncertainties

in the brightness of new stars are introduced by the calibration process. Among the possible methods for determining the best amplitude estimate are simple averages or weighted averages. The simple average amplitude estimate is

$$A = \frac{1}{N} \sum_{i=1}^{N} A_i \qquad 3.4\text{-}1$$

Where the A_i are the N individual measures. When N is small and the calibration is a single measurement on each of several standard sources, this is the best amplitude measure. However, when the calibration of a particular detector against a particular star is repeated several times, then knowledge is obtained on the characteristic probability distribution function, $p_j(A)$, for each detector j. Then the best amplitude estimate is

$$A_j = \sum_{i=1}^{N} A_{ij}\, p_j\,(A_i) \qquad 3.4\text{-}2$$

However, it is uncommon for the unknown star to be surveyed repeatedly by the same detector. Then more complex information is needed on the probability distribution over all detectors, and

$$A = \sum_{i=1}^{N} \sum_{j=1}^{M} A_{ij}\, p_j\,(A_i) \qquad 3.4\text{-}3$$

The establishment of the complete probability density function is, of course, a major responsibility of the survey calibration. The above relations 3.4-1 can be further complicated by the

inclusion of the known information on the certainty of each measurement. Since, in general, this S/N value is available for every detection, it too can be included as a weighting factor in 3.2-3 so that.

$$\langle A\rangle' = \frac{1}{\sum_{i=1}^{N} (S/N)_i} * \sum_{i=1}^{N} \sum_{j=1}^{M} A_{ij} (S/N)_i \, p_j (A_i) \qquad 3.4\text{-}4$$

where the first term is the normalization factor for the (S/N) weights.

The relations 3.4-1 to 3.4-4 serve to decrease the uncertainty of an amplitude measure in a statistical sense by making a best estimate average. If p(A) is gaussian or nearly so, then the multiplicity of measurements gives a photometric accuracy improvement over the single measurement uncertainty of a factor of $\sqrt{N}$ for the average amplitude. Thus, a 10% photometric accuracy can be achieved by 4 measurements of 20% error or 25 measurements of 50% uncertainty.

The positional weighting problem occurs because of a non-uniform spatial distribution in source location. The primary cause of the non-uniformity is the typical use of double-staggered arrays of detectors so that a portion of the sky is measured by two detectors with adjacent portions covered by only one. Typically, the singly covered strip is twice as large as the doubly covered one, and it is difficult to locate additional scans with sufficient accuracy to place a second or third scan

in the singly covered region, thereby recovering uniformity of coverage. The probability distribution across the overlapped and non-overlapped portions of the detector is the product of a uniform distribution in each section times the normalized energy distribution function of the star image.

If point sources are assumed, the energy distribution can be given by the diffraction limit distribution of:

$$I(\rho)= \frac{I_0}{(1-\varepsilon^2)^2} \left\{ \frac{2J_1(ka\rho)}{Ka\rho} - \varepsilon^2 \left(\frac{2J_1(k\varepsilon a\rho)}{K\varepsilon a\rho}\right)\right\}^2 \qquad 3.4\text{-}5$$

where ε is the radial obscuration factor, ρ is the radial coordinate of the diffraction paitern, $k = 2\pi/\lambda$, a is the aperture radius, and I_0 the central peak intensity of the diffraction pattern. This is normalized by the integral of $I(\rho)$ over all ρ. Note that 3.4-5 is a function of wavelength. When a broadband filter detector system is used, the energy distribution is given by the integral over wavelength of 3.4-5 times the filter function F(d).

For non-diffraction limited optics, other intensity functions can be used as given in Born and Wolfe.[11] Since each source has a positional uncertainty in cross scan given by the product of the uniform distribution and 3.4-5, and a similar uncertainty product in the scan direction, the combination of multiple detections implicitly assumes an adequate overlap of the individual positional uncertainties. In previous programs, the

distribution functions were assumed to be sharp, rectangular boxes corresponding to the detector instantaneous field of view for each detection. This proved to be adequate for combining detections but involved some care in implementation in the software because, in general, no corner of one box fell inside the second box. For survey missions of higher sensitivity, such an approximation must be examined carefully to develop the best combinational approach to multiple overlapping positions. The complexity of convolving third, fourth, or further measurements adds yet more difficulties. The convolution must be done with care if the multiplicity of measurements is to reduce the uncertainty measured position while providing multiple detection confirmation. Further, the time-to-position transformation for each scan introduces a third level of uncertainty for multiple scan combinations.

The most complex weighting problem for large IR surveys is the determination of a confidence measure for each source, given multiple measures in (possibly) multiple spectral bands. The task is more difficult than even the combination of all the measurements since the survey data has reference to other surveys made in similar wavelengths and in other parts of the spectrum. The wide variation in noise and sensitivity from detector to detector and from measurement to measurement must be accounted for. The origin of the various multiple measurements does allow a reasonable separation of the combination task into a series of combinations. The sequence presented in Figure 4 (Section 3.1)

indicates a possible ordering of the several combination steps.

The first level of multiplicity in detection occurs in the focal plane at step 7. Combinations here account for the overlap of detectors and the matching of the multiple detector scans. Lacking external knowledge of the spatial extent of a detected source, signals occurring on two adjacent channels are attributed to a single source if the signature on each detector is essentially point-like. (See Section 4 for non-point objects.) Then, if a time spacing between measurements is within the bounds set by column spacing, scan rate, and associated uncertainties, the source is assumed to transit the region of overlap between the two detectors. Such a pair of measurements is then combined in amplitude, its positional uncertainty assigned to the overlap region, and its confidence determined as described below for combining S/N values. If detections of proper time spacing occur in other colors in the same detector row or rows, then the multiple color measurements are assigned to a common position, retaining the separate amplitudes in each color. Naturally, this multiple color combination occurs after detector overlap testing.

Within a single scan, the combination of focal plane characteristics is done in the time domain. This prevents positional uncertainties associated with the sensor pointing history from affecting the combination success and error rates. For

independent scans the combination of repeated measurements necessarily occurs in a celestially fixed coordinate frame. It is intuitive that the time-to-position transformation must be done carefully to maintain the minimum error box size.

For two independent measurements the best combination of information occurs in a co-adding sense. That is, the peak signals and the square noise variances are combined and used to produce a new S/N value. Measures of the signals and noises in common units must be retained to make this combination properly. The new S/N is given by:

$$(S/N)^1 = \frac{S_1 + S_2}{(N_1^2 + N_2^2)^{1/2}} \qquad 3.4\text{-}6$$

where the subscripts 1 and 2 refer to the first and second signal S and noise N. Generalizing 3.4-6 for n-tuple measurements,

$$(S/N)^1 = \frac{\sum_{i=1}^{N} S_i}{\left(\sum_{i=1}^{N} N_i^2\right)^{1/2}} \qquad 3.4\text{-}7$$

The reader should recall that the MSD noise is calculated so that the N^2's are immediately available; then the square of the new S/N is found by squaring the sum of signal values and dividing, thus saving a slow square root operation in favor of a faster multiplication.

Two extensions to the above algorithm can be made. First, the non-detection of a source at a given position is automatically handled by setting one of the S_l's to zero. This will tend to underestimate the $(S/N)^l$ value since the signal could have been as large as K times the rms noise and still not be listed as a front-end detection. K is the threshold level at the first detection algorithm. Second, 3.4-7 can be extended to include weighting factors based on the sensitivity of each detector. Since the lth detector could have a sensitivity different from the average, the l signals in the numerator of 3.4-7 can be multiplied by $R_l/\langle R\rangle$ where R_l is the responsivity of the lth detector and $\langle R\rangle$ is the average responsivity. More complex forms of the detection probability function can be used if sufficient information exists to describe Pd(i).

When the additional measurements are in different colors, special care must be used in combining the confidence measures. The spectra of the source is not flat over the wavelength bands covered by the detector system. That means that different classes of sources will have different ratio responses in the multi-color measurements, and the ratios will depend in part on the relative sensitivities of the wavelength bands. This immediately suggests a weighting factor for combining the S/N ratios. A table of color ratios versus temperature can be created by convolving a black body spectrum at each temperature with each filter-detector combination. Entries in such a table are used to give a weighting factor for each color band based on

the source color temperature which is then used to combine the respective S/N values analogously with 3.4-7. (This seemingly circular calculation can be achieved in practice by using the already calculated amplitude estimates to determine T_c, which is then used to weight the S/N values.)

3.5 False Source Algorithms

During other survey programs a number of phenomena were identified which produced detectable signals. These were initially identified as potential sources, but inspection of the data records revealed some unusual characteristics. Analysis indicated that several mechanisms produced false signals which were so unique that they could be fully eliminated from the data. Cosmic rays and other ionizing particles produced characteristic rapid rise signals; dust particles exhibited a typical out-of-focus doughnut covering many detectors, and off-axis Earthshine produced azimuthally correlated extended objects.

Figures 5 and 6 illustrate radiation particle hits. These events ionize the detectors, often saturating the conduction band and produce signal pulses characteristic of the impulse response function of the sensor electronics. If the signal were examined at the output of the detector amplifier, such pulses would be nearly delta functions with a duration governed by the time necessary for the bias supply to drain off the ionized electrons. This time is characteristically milliseconds with

rise times of the order of microseconds per volt. The electronic bandpass filters degenerate this sharp spike to the illustrated signal. The rapid rise of these signals is preserved well enough to distinguish large pulses from real sources very easily, however, and rise slope has been used in many programs to identify such spikes. Some confusion occurs when the spike heights are smaller because the sampling rate begins to confuse the rise slope calculation. Typical spikes reached peak or A/D limiting value in 2 to 4 samples whereas the sharpest point sources covered 8 to 10 samples before reaching its peak.

Analytical models of the radiation particles have indicated a spectrum of potential pulses should be seen by these IR detectors to much smaller amplitudes than actually experienced. This could be caused by failure of the slope discrimination algorithm for small amplitudes or by inaccuracies in the model. However, if small spikes are missed by the algorithm, they will likely remain in the data lists because they appear as high S/N sources. Multiple observation tests must be carefully arranged so that a single large S/N signal cannot pass in order to avoid this problem.

Figure 5 shows a second difficulty of particle events. Typically, their electrical signals are strong enough to cause significant crosstalk signals in other detectors. Since these have been doubly band filtered, the crosstalk signal looks much

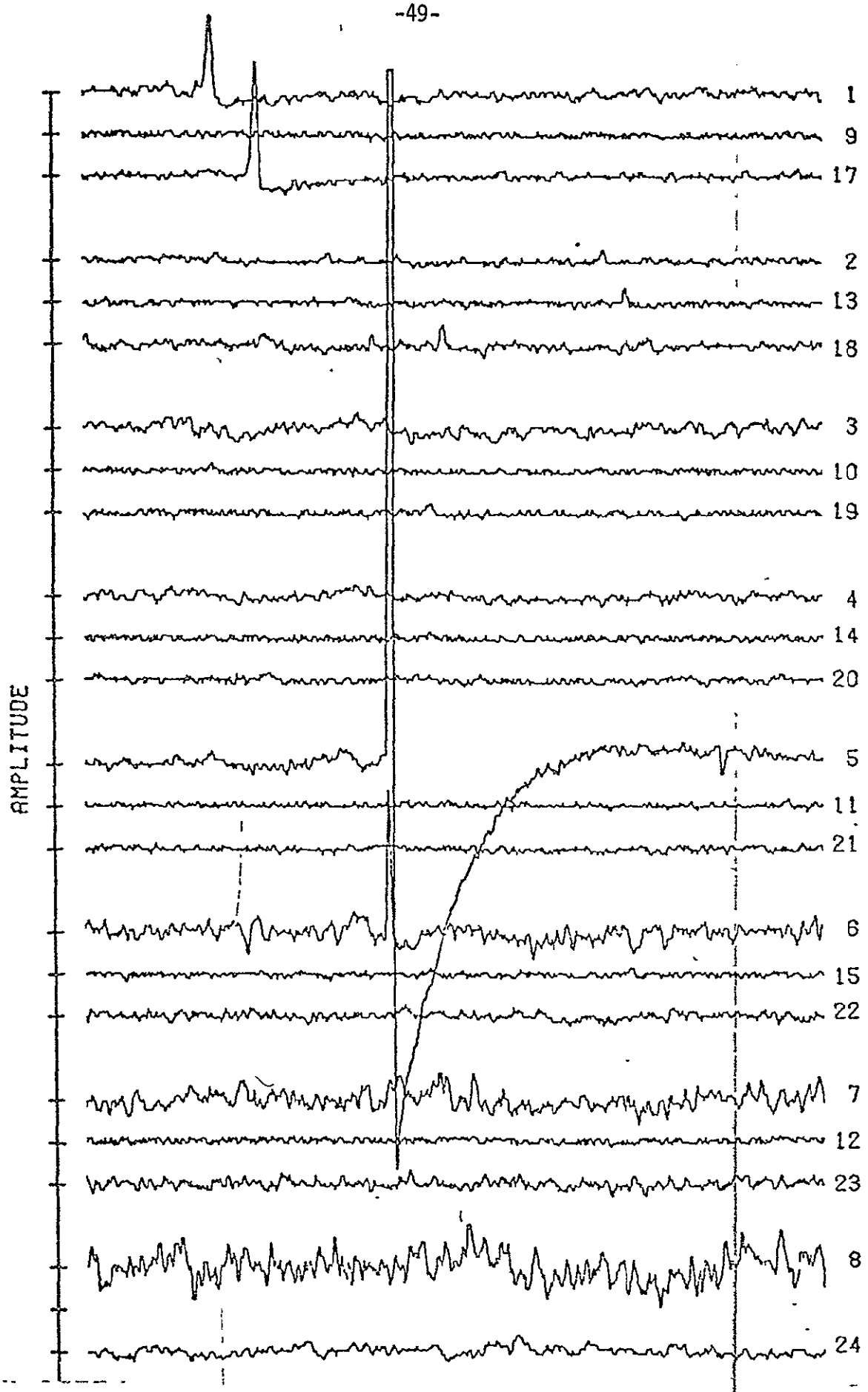

Figure 5. Sample Data - Radiation Spikes with Crosstalk

more like a real source than the original radiation event. However, these are easily identified by their time correlation with the particle event. If the signal times of eliminated spikes are retained, then the crosstalk signals can be tested for and eliminated.

Figure 6 illustrates the characteristic signature of a dust particle. Since the particle is very nearby, the image is severely out of focus producing an image in the focal plane of the illuminated primary mirror with the central spot darkened by the secondary mirror system; the size of this doughnut depends on the distance to the dust particle. Because the image is out of focus, each detector is typically fully illuminated by the particle. Simple radiation balance calculations give an equilibrium temperature of around 270°K for these particles illuminated by Earthshine (all observations were made in the sun's shadow) so that the 4 micron band has very little energy and the 20 micron band is most strongly excited as the figure illustrates. The image's double hump and the low color temperature are the characteristics which allow simple discrimination algorithms. One must be sure to check all possible channels for time coincidence signatures as well since the detector which transits the edge of the doughnut will have only a single hump signature.

Another type of false source is the nonstationary space bodies. These include Earth satellites, planets, asteroids,

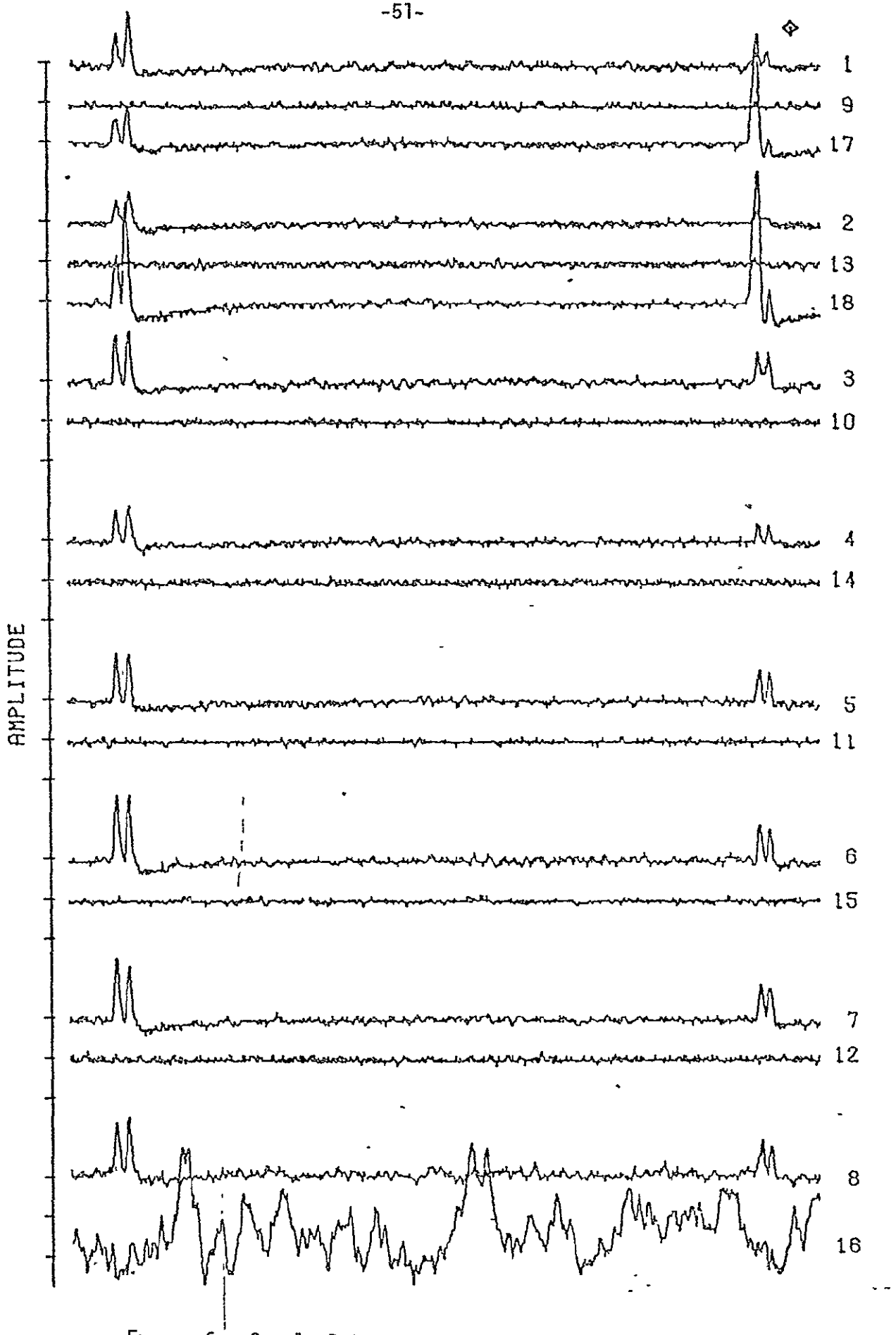

Figure 6. Sample Data - Dust Particle Signatures

meteors, and comets. The planets are readily identified because of their known positions. The caveat that the planet's location at the time of observation must be known applies. For the outer planets the proper motion is very small, and observation time is not critical. For the closer ones, however, over the course of a year-long survey, the total motion will be significant, and the varying viewing aspect due to the sensor's orbit must be accounted for. More difficult to deal with are the 1200 known asteroids since their orbits are not accurately determined in all cases. Even worse, extrapolation of the known asteroid population[12] indicates that tens of thousands of completely unknown objects could possibly be seen by a very sensitive infrared system. A great body of science can be recovered, however, if the motion of these discovered asteroids can be used to determine orbital elements; the resulting distance knowledge allows determination of albedo and size parameters for the asteroids.

The most difficult moving objects to deal with are Earth satellites. The large number of these presents a formidable difficulty, and their very rapid relative motion compounds the problem. However, a good deal of these sources have known orbits reducing the task to checking the lists for potential identification. However, the positional computations involved are not trivial. Satellites in nearly synchronous orbits could be a greater problem because their relative motion will be smaller. As with the asteroids, a major task will be the

association of a given observation with an object seen in a previous observation. If the lists of possible moving objects (that is, all large signals seen only once in a given position) are large, it may be difficult to trace a single object's motion from observation to observation.

4.0 DATA PROCESSING FOR EXTENDED SOURCES

In contrast to the thorough analysis of techniques, background, and algorithms described in Sections 2.0 and 3.0 for point-source surveys, very little is understood of the data processing task for extended objects. As discussed in Section 2.4, this includes objects which are slightly larger to very much larger than the detector resolution. In some ways the desired results are similar to the point-source cataloging of Section 3.0, but in others the task is totally different. This section will discuss first the extended objects which are similar to point sources, then the wide field sources, their resulting final products, and the approach to processing them.

4.1 Slightly Extended Objects

SEO's are not much different from point sources. In general, their characteristic signatures are only perturbations of a point-source signal. Typically, they will be seen in only one or two detectors, and the signal will be two to three times longer in duration than point sources. Photometrically, their edges can be as sharply defined as point sources so that the upper frequency limit of their signal is the same as point sources; their lower frequency is only 10% to 30% lower than the point source and is due only to the increase dwell time caused by a source image a few times larger than the blur circle. Physically, these objects are associated with large circumstellar shells and bright knots in HII emission regions.

Detection of SEO's can be done exactly the same as point sources if the increased dwell time is allowed for. One possible approach to this is to use a double correlation model matching the characteristic rising portion of the signal separately from the characteristic falling portion. The variable spacing between these two edges then gives a measure related to the sources angular extent. Another method is to use point-source correlation, but simultaneously test the peak signal-to-noise ratio. Then a source with a high enough S/N value but a low correlation coefficient would indicate the presence of an extended object, and measurement of the pulse width would be related to the angular extent.

For best performance, the detection routine for SEO's should use a digital filter matched to the bandwidth of the source's signature. This filter would be similar to the point source's but of slightly larger angular extent. The upper frequency limit is determined by the duration of the SEO pulse. If a point source produced a rectangular pulse of duration τ (equal to the dwell time on the detector), the power spectra would have its first zero at a frequency f_0 of $1/2\tau$. Then an SEO with a dwell time of $\tau(1+\varepsilon)$ would have a lower cutoff frequency of $f_0(1-\varepsilon)$.

Once the SEO has been detected and a value assigned to its extent, the source can be treated just as a point source measurement. The criteria for multiple observation and reasonable spectral matching and brightness determination follow point-source

requirements exactly, except that the positional uncertainty is increased due to the size of the source. Since these objects will not (by definition) cover more than two detectors, the cross-scan position error is relatively unchanged, but the scan error should increase by roughly the angular size. The SEO's are assumed to have sharply defined edges and reasonably uniform brightness distributions across their discs; some error in determining their size results from such limitations, so it may be worthwhile to approximate the size of these objects in quantized steps. That is, if the size error is ±3 arc minutes, then SEO's could be given as 0, 3, 6, 9, 12, ... arc minutes. This approach would save some computation time over calculating the individual size to one or two digits without losing information.

4.2 Photometric Mapping

For truly extended sources, the brightness distribution of the source determines the resulting data signature. The analysis of this data intends to recover the spatial variations in brightness and present it in a readily understandable manner. The two most common presentations are contour maps of the brightness and photo images. The contour map has the advantage of being easily quantized, while photo images are more useful in understanding variations near the resolution limits of the survey. The techniques of producing these products are in widespread use on a number of other programs, the method to gather and process the initial data is much less understood.

Because it is easily quantized, contour mapping is the most commonly used data product for infrared and radio surveys. Data input for these measurements is typically from beam switched telescopes with the two beams aligned with an individual scan line and multiple adjacent scan lines made over an extended emission region. The individual scans are essentially sequences of difference measurements. These sequences can be algebraically inverted to produce the brightness values along the scan line with some errors introduced by the inversion process due to the D.C. instability of the numerical inversion. The effective resolution element is typically somewhat larger than the beam size due to these instabilities. Multiple adjacent scans then give an array of local brightness measurements which is then used as input to standard contour plotting routines.

Photo image processing is a powerful analysis tool not used extensively in astronomical studies but common in planetary investigations. Using the same array of brightness elements as described above, a photo image is produced by converting each brightness value to a grey scale (or a color scale) value on a printing device or a cathode-ray tube. Using multiple strike-overs an eight-level grey scale, for example, can be produced on a standard line printer using the algorithm below.

		Grey level →							
		1	2	3	4	5	6	7	8
	1	b	-	=	+	X	X	0	0
Overstrikes	2	b	b	b	+	X	X	X	M
↓	3	b	b	b	b	b	=	*	W
	4	b	b	b	b	b	b	b	#
Results			-	=	+	X	[illegible]	[illegible]	[illegible]

The greatest difficulty in using photo image representations of the data is that each individual element is commonly not an independent brightness measure. Rather, it is overlapped by the information of adjacent elements, a result of both the measurement technique and an artifact of the data recovery algorithms. The resulting image rarely has the resolution implied by the beam size of the system, and the photo product appears to have very low contrast. A number of techniques have been devised for planetary image processing to improve this situation. These techniques generally tradeoff the photometric accuracy of the image for the spatial resolution desired. Thus, photo images are a supplement to contour maps of source intensity, not a replacement. The algorithms to be used for contrast enhancement and for resolution enhancement will be reviewed in phase 3 of this study; these will be adaptations from similar current efforts in image processing.

A more difficult problem is the creation of the array of intensity measurements. Survey instruments typically do not use beam switching, relying instead on spatial scanning to

modulate the signal from the infrared detectors. The outputs are bandlimited in frequency to avoid the difficulties of D.C. drifting so that the information of the wide-scale intensity distribution of a source is lost or at best compressed severely. Successful mapping of extended regions requires that the information content at the frequencies corresponding to the desired spatial extent be restored. It is immediately apparent that the measurement technique has performed a spectral compression of the spatial image. It is thus necessary to understand the compression function and successfully invert it to recover the desired intensity data. Very little is currently understood of the scope of this task and the potential limitations; candidate techniques for this inversion are either algebraic or an application of orthogonal transformations.

Algebraic restorations are the simplest to implement. Given the transfer function of the scanning telescope system, the (digital) difference equations can be written, as described in Gold and Rader[9] and in Section 3.0 of this report. Then the n equations relating the several input and output samples are algebraically inverted to express the input values as a function of output samples. This system is then incrementally solved given the detector's sequence of Y_1 measured output samples. Several difficulties arise with this approach. Since the algebraic inversion is based on the ideal transfer function, there are inherent limitations in the accuracy of the restoration due to a

misfit between the actual system and its model transfer function. Further, the algebraic methods are inherently unstable in the presence of noise.[13]

Since the A.C. coupled transfer function typically has zeros at zero frequency, the inversion will have unstable poles at zero frequency. This D.C. instability will require iterative fitting of short scan segments with the D.C. value of each end defined (or at least assumed). The task is the digital equivalent of the solution of a non-linear differential equation with defined boundary conditions, a formidable task. This is further complicated by the effects of digitization which necessarily introduce at least a one-bit uncertainty in the lowest frequency of the system data which drives the D.C. instability. Coupled to this are the effects of inverting wide-band noise and the algebraic method becomes almost untractable. It is difficult to envision a successful inversion unless the signal is so large that noise can be smoothed out (a form of severe high frequency filtering) and digitizer uncertainty becomes negligible. In such a case, however, the spatial resolution of the system is degraded by the smoothing.

The difficulty of using a direct inverse of the transfer function can be seen as follows. The sequence of output values r_m are related to the noise n_m and the object's intensity distribution O_n by the transfer function h_{nm}. That is:

$$r_m = \sum_{n=1}^{N} h_{nm} O_n + n_m \qquad 4.2\text{-}1$$

The inverse of this, using M=N observed samples is in matrix notation:

$$\vec{O} = [h]^{-1} \vec{R} - [h]^{-1} \vec{N} \qquad 4.2\text{-}2$$

Now if $\overline{N}$ is an unknown random function, then the second term in the r.h.s. of 4.2-2 is the error in reconstructing the original intensity distribution. Since most transfer functions are simple, [h] is mostly zero, with small elements near the diagonal, so that $[h]^{-1}$ has many large elements. Then for samples with finite noise n_m, the error in reconstruction is still randomly distributed but very large. An example by Phillips[13] with an input signal plus noise, S/N > 2000 was reconstructed to a S/N' less than 3.

A potentially more successful approach to the task involves the use of orthogonal transformations. Essentially, the scan matrix is transformed to a domain which allows some separation of the noise and digitizer effects from the data. The data is then weighted to recover the low frequency information and re-transformed to the original domain creating the intensity array. This is then mapped by photo imaging or contour plotting and analyzed. This approach is commonly used in television image compression codes where the compression and recovery are externally controlled. In the survey problem, our goal is to discover the original compression code and invert it with the

minimum error. Transformations which have been successful in such applications include Fourier and Hadamard methods and Karhunen-Loeve transformations. The latter are probably optimal in the sense of minimim least-square errors in the ultimate results, but except for simple (and thus limited) approximations are unwieldy to implement. Since the Discrete Fourier Transformation is a limiting case of the Karhunen-Loeve transformation for independent data, it is intrinsically attractive. The forward DFT is given by

$$F_k = \frac{1}{\sqrt{N}} \sum_{0 \leq n \leq N-1} f_n \exp(-i2\pi nk/N) \qquad 4.2\text{-}1$$

and its inverse is:

$$f_n = \frac{1}{\sqrt{N}} \sum_{0 \leq k \leq N-1} F_k \exp(i2\pi nk/N) \qquad 4.2\text{-}2$$

where the input data sequence is $(f_0, f_1, \ldots f_{N-1})$ and the transformed data are $(F_0, F_1, \ldots, F_{N-1})$. The transformed sequence is naturally ordered by the index k, with increasing k corresponding to higher frequency components. The Fast-Fourier Transformation (FFT) is an efficient method widely used to compute the DFT as given above.

4.3 Detection of Extended Emission

The previous section considered the problem of recovering the spatial intensity information for extended sources. Since a significant portion of the potential objects is known a priori,

the major difficulties are in the reconstruction. It is assumed that the scan data is made available for the full known extent of an object such as the galactic center and that data is treated to recover and map intensity distribution. A second problem exists for those objects which are not known as extended emission regions in discovering them. Of course, it would be possible with unlimited computing resources to recover the entire intensity over all the sky and then "discover" unknown emission from the resulting all-sky map. However, for surveys designed to gather stellar information as well, the instrument's limitations imply a sacrifice of some extended source capability. With limited resources and compromised data, a more worthwhile approach would be to identify the region in the unprocessed survey data and then map the limited area of interest.

This task is not as difficult as one might suppose from extrapolating the point-source detection problems. The mapping algorithms are intrinsically limited in the accuracy of the recovery by noise and instabilities which implies constraints on the dimness of the extended source (or the strength of spatial intensity gradients), on its upper size limit, and on the achievable resolution. Generally, the mapping procedures will require peak-to-rms S/N values of 20 or more over regions not exceeding 10 degrees. As long as the sensor electronics do not exhibit D.C. drifting over a comparable range, a simple peak detecting algorithm measuring

the local mean signal in a window larger than ten degrees should discover most of the unknown regions which are mapable with a survey instrument. Section 3.0 covered the algorithms applicable to the peak detection task.

5.0 DATA PROCESSING SYSTEMS

There are a number of ways to implement the survey data processing scheme described in Sections 2.0 through 4.0, depending on the facilities and resources available and on the operational constraints. Previous survey programs have generally had unrelated observing and data processing schedules with the data reduction taking four to twenty times as much total CPU computer time as the sensor's observing time. For example, processing the data collected on three 100-minute orbits of the CMP sensor required over 120 hours of computer time on an XDS-Sigma 7 machine. On the other hand, the massive tasks of the IRAS mission allows only 18 months to process 8 months of data, including the generation of many final products (catalogs, overlays) not involved in the CMP effort. The tremendous consumption of CPU time in previous programs indicates a need to organize an IR data processing system with care. The following sections describe a basic division of the processing task into two sections, the front-end detection and the back-end cascade, and a number of parallel monitoring functions. This structure is dominated by the point-source processing requirements which are well understood. The extended source mapping is roughly a parallel function with the interaction points indicated in the flow diagrams.

5.1 Overall Computing Structure

Figure 7 diagrams the suggested processing flow structure; this is just a formalized grouping of the processing tasks discussed

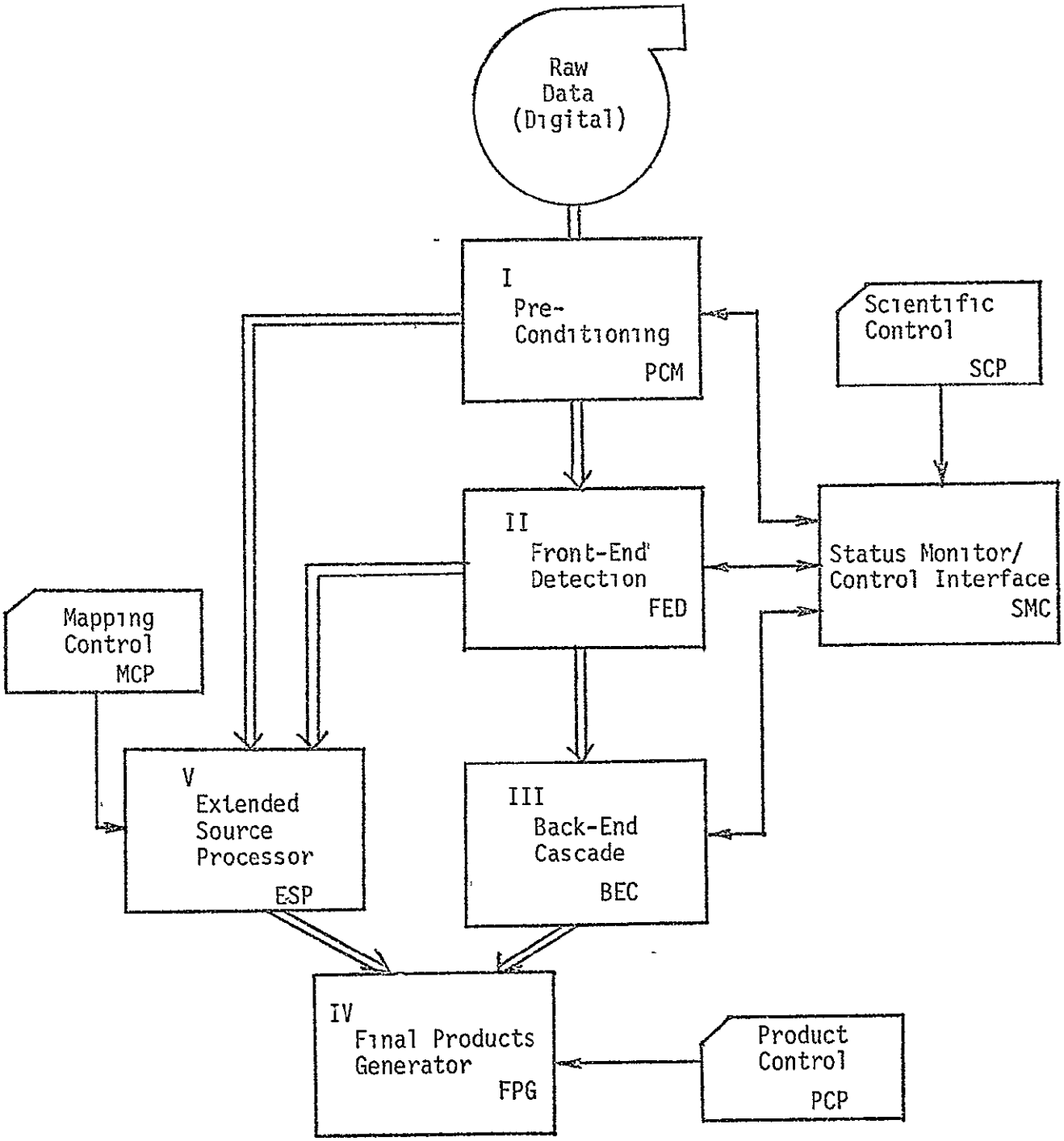

Figure 7. Computing Structure

previously. In the software packages, the pre-conditioning front-end processor and part of the monitor functions can be combined to form a single executing program. The back-end cascade and remaining control/monitor functions form a second operating package which can run off the data tapes' output by the first package. Final products generation is best run as a third independent group since the interaction within this package is dominantly based on graphic and publication requirements, not on scientific decisions. The first group processing is generally run as a fixed operation designed to extract the statistically maximum amount of information from the data stream, control of these functions is based only on system load requirements. The scientific decisions interface with the processor flow in the second group, where tradeoffs occur to maximize the quality of the data products. The extended source processing is a fourth software package which uses the pre-selected data output by the pre-conditioning phase to map known regions of interest and the data on newly detected objects from the front-end processor.

In small-scale surveys, each step of the sequence of Figure 7 can be executed sequentially for the entire data block. For larger surveys the several steps would be running in unison as the data from each step was processed and passed on to the next.

For very large-scale processing tasks, the operation can be split into five distinct packages with the pre-conditioning

being separated from the front-end processor. This would allow the use of multiple dedicated computers or a large-scale parallel processor to continuously execute all the data phases. In this way the later stages can process data as it becomes available from the preceding level. Especially advantageous in this case would be the use of hardware processors dedicated to specific tasks within each group. For example, the basic noise block calculation could be done by a special CPU in the pre-conditioning. Likewise, a dedicated correlation processor for the multi-channel data could be performing the data transformations to convert the raw data stream to optimally filtered or correlated data streams. Another processor would then monitor these outputs and the noise data to operate the detection function. Micro-coded hardware processors can operate at very high speed if their computing task is sufficiently limited; by using separate processors for each basic task in the pre-conditioning and front-end detection packages, a very high throughput can be achieved. A supervisor computer could perform the monitor and control operations for the two primary phases and channel the final outputs to disk or tape storage devices for access by later stages.

Once the data has passed the front-end stage, multiple processing is no longer attractive since the purpose of the third and fourth stages is to condense the mass of data into an ordered catalog. This task requires sophisticated decisions

for data combination making a general-purpose computer more attractive. This is especially true for the final products phase where high-level, high-speed graphics are required. The mapping routines of the Extended Source Processor also require the power of a large and versatile computer. The overall processing system could consist of an array of high-speed special hardware processors controlled by a dedicated mini-computer. This would feed data to storage devices which are accessed by a large, general-purpose computer. The remaining processing would be done by software packages on this machine feeding the final outputs to the appropriate storage devices.

Monitoring functions performed in the first stage by the mini-computer can feed real-time interactive devices. This would allow the data processing scientists to discover flaws and problems in the data quickly enough to make corrections before excessive processing time is consumed. In previous programs this interactive analysis was done by repeated batch processing on a large computer, with several hours of CPU time commonly consumed before the unexpected characteristics of the data were understood and accounted for in the software. Further, each new set of data required more interactive processing. By replacing this multi-pass processing with an interactive facility, a sizable portion of the CPU consumption can be saved.

With the prior understanding of the data quality, the monitor functions of the later stages can be reduced to sample

checking of the results of each decision level. For example, foreknowledge that a block of potential sources came from low-quality data would allow the scientist to alter a decision gate to prevent an excess false source rate. While this control could be done automatically, the software required would be complex and consumptive of processing time. By allowing qualitative decisions to be made externally, the most complex decisions are removed from the software requirements. All that the monitor programs would have to do is provide enough quantitative measures and displays to allow the judgments to be made accurately. Since each stage of the processing reduces the size of the data base, the need for real-time interaction fades; it becomes feasible to rerun a processing step in the back-end phase when difficulties are encountered where this would have hampered processing severely during the initial phases.

5.2 Front-End Processing Flow

The data pre-conditioning and front-end detection phases and their monitors comprise the front-end processor The inputs to this group are the raw survey data and the pointing ephemeris, and the outputs include tapes of the extended source data blocks, noise records, and two groups of detected sources. The detections are separated into categories which can be judged solely on their individual signatures as false signals, such as dust and spikes, and real signals from potential stars. Also output are the summaries of the monitor and control functions

and any records of housekeeping data from the raw data tapes. Hardware implementation of the front-end phases can be used to minimize the stretch of processing time over data gathering time; software approach can also be used in whole or in part saving hardware costs but probably increasing computing time.

The pre-conditioning task converts the packed integer telemetry data into usable form. The data are unpacked and grouped as streams of samples from each detector and each housekeeping function, the voltage compression is inverted and offsets removed, and the initial data monitoring task is performed. This includes the tracking of record gaps and any operational variations indicated in the housekeeping (such as a detector turned off). If the PCM digitizing system produced a data quality measure (typically telemetry signal strength), this is monitored for interactive decisions. Preliminary calculations of the noise are done for each block of data, time tags are calculated, and the data passes to the front-end detection phase. Interactive monitoring of this phase allows judgment of the quality of the digital records so that bad tapes or inadequate telemetry can be discovered as early as possible.

The front-end detector performs the first complex calculations on the data; its associated monitor routines produce the earliest judgment on the sensor's performance, and a quality measure of the survey data. Side calculations from the sensor pointing ephemeris determine the time boundaries of

desired extended source data, and the raw data for those areas are written on the extended source tapes. The data streams from each channel are transformed to optimally bandlimited and correlated sequences. These three sequences are processed by the detection routines, and data passing the detection screens are measured. These sources are written on either the false source or potential star tapes for access by the later processing stages. The remaining noise calculations are made and written on the noise record with enough data to determine why a source was not detected at a particular time if it is detected later in the same spatial position. The remaining front-end monitor functions produce noise spectra for analysis, summaries of the false sources, status of the self-adapting detector routines, and possibly sample plots of the raw or transformed data for visual study. The control function here allows a statistical evaluation of the survey instrument performance, and records the judgment of quality or confidence to be used during later processing stages. Various levels of noise analysis are performed using both the raw data and the transformed sequences to generate noise frequency spectra and other analyses for occasional study. The spectra should include data containing real sources, false sources, and noise only and at various signal levels for the first two so that complete understanding of the data will be available.

5.3 Back-End Cascade

The middle processing phase is called a cascade because of the waterfall-like effect of the data flow. As more data is

gathered by the sensor and observations are repeated at various levels of redundancy, the sources move from the raw master source file of Figure 8 to the final data base. Each cascade level monitors the planned and the actually executed observing schedule qualifying sources for the next level as sufficient data is gathered. Both moving sources and fixed position variable sources must be accounted for so that in addition to reducing the data base, a number of auxiliary data bases are generated. Interactive processing of the data is less needed here, but the status reporting function of the supervisor programs increases.

The organized sequence of the back-end cascade and its computations were discussed in detail in Section 3.0. The most important addition to the back-end routines in the overall system is the monitor and status programs. Each cascade level must be monitored since the gate adjustment will best be done by qualitative analysis of the output. Naturally, re-processing of some gate levels will be needed, and a means of saving the discards of each cascade will save time if that step must be redone. However, this requires a significant amount of redundant storage since the entire body of data will end up being saved three or four times. Scheduling of the cascade processing can reduce this storage overhead if attention is paid to the repeat-observation schedule of the sensor. Knowledge of data quality variations which was generated in the front-end phase also reduces the re-processing requirements once the functional effect of gate level variation is understood for each gate.

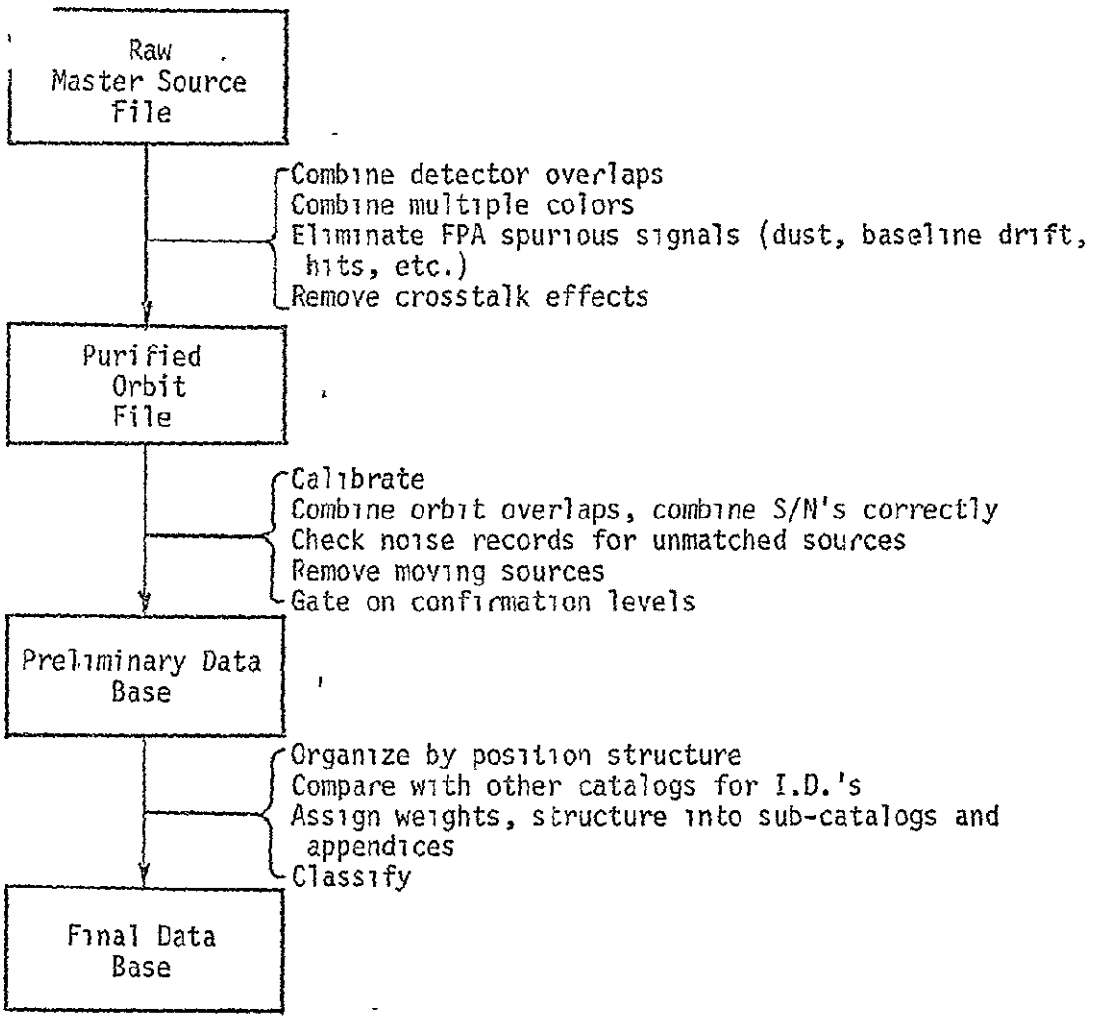

Figure 8. Back-End Cascade Structure

ORIGINAL PAGE IS
OF POOR QUALITY

The final products generation can be considered the last step of the cascade sequence. Rather than further deleting unqualified data from the master data base, however, this processor phase subdivides the data into desired categories. For example, a master catalog of stars observed is commonly produced using the best estimate values for position and brightness and computing the correlations of this catalog with other source catalogs. Subclasses of this catalog may list the observation sequence and possible parameters of variable sources, an extended source catalog, or lists of sources with specified spectral characteristics. Monitor functions of this final step describe the completeness of the several catalogs as the survey processing progresses.

5.4 Extended Sources and Survey Calibration

As discussed in Section 4.0, the techniques needed for extended source processing are significantly different from point-source procedures, a fact determined largely by the difference in final products. To produce large-scale maps of these regions the raw data from many scans must be combined and transformed to an array of D.C.-like brightness values. This array is then transformed into a graphic image or contour map of appropriate scale. Routines which remove point sources from the data may be desired, and other routines which put them back on the maps may also be needed. For smaller extended sources, integration of the total brightness might be performed and the source included in the master catalog with an indication of the size of the region. The software routines for producing contour maps are readily available. Similarly, routines for producing photo images can

be modified to suit the resolution capability of the survey instrument.

Calibration of the star survey is another major problem which falls outside of the main data processing flow. Only in a carefully designed observing program can the calibration be done completely separate from the survey itself. For example, the IRAS mission is planned to observe a small set of standard stars once or twice per orbit; all measurements during the following orbit would then be calibrated by these measurements. In other survey programs, however, the standard stars and the survey itself were mixed together on every scan with some of the observations of known stars being called "standards", the others "unknowns." The voltage measurements of these standard stars are fit to their defined brightness in a least square sense to produce calibration factors for the detectors. Monitoring of these standards must be done at all levels of the processing scheme so that any long-term variations in the calibration can be discovered and so that the final catalog values are truly best estimates of the actual source brightness. Difficulties arise with this technique when the system responsivity varies during the survey since no single calibration star is normally observed often enough to monitor the variations.

6.0 REFERENCES

1. Neugebauer, G., and Leighton, R. B., 1969, NASA SP-3047.

2. Low, F. J., 1973, AFCRL-TR-73-0371.

3. Low, F. J., Kurtz, R. F., Vrba, F. J., and Riecke, G. H., 1976, in press.

4. Price, S. D., 1976, Proceedings of AIAA 4th Sounding Rocket Technology Conference, Boston, MA.

5. Walker, R. G., and Price, S. D., 1975, AFCRL-TR-75-0373.

6. Price, S. D., and Walker, R. G., 1976, in press.

7. Whalen, A. D., 1971, Detection of Signals in Noise, Academic Press, New York.

8. Gerlach, A. A., Theory and Applications of Statistical Wave-Period Processing, 1970, Gordon and Breach Science Publishers, New York (3 volumes).

9. Gold, B., and Rader, C. M., 1969, Digital Processing of Signals, McGraw-Hill Book Co., New York.

10. Rader, C. M., and Gold, B., 1972, p. 43, in Digital Signal Processing, Rabiner, L. R., and Rader, C. M., ed., IEEE Press, New York.

11. Born, and Wolf, 1970, Principles of Optics, 4th ed., Pergamon Press, New York.

12. Murdock, T. L., 1973, AFCRL-TR-73-0154.

13. Phillips, D. L., 1962, J. ACM, 9, 84.

14. Huang, T. S., ed., 1975, Picture Processing and Digital Filtering, Springer-Verlag, New York.

15. Sedlmeyer, Axel, 1974, Structures for Wave Digital Filters, D. E. thesis, Ruhr-Universitat Bochum.

16. Javid, M., and Brenner, G., 1963, Analysis Transmission, and Filtering of Signals, McGraw-Hill Co., New York.